 doi:10.20944/preprints202012.0565.v1

Article

The effect of Ni-Modified LSFCO Promoting Layer on the Gas Produced Through Co-electrolysis of CO_2 and H_2O at Intermediate Temperatures

M. Lo Faro[1]*, S. C. Zignani[1], V. Antonucci[1], and A. S. Aricò[1]

[1] Institute of Advanced Energy Technologies (ITAE) of the Italian National Research Council (CNR), Via Salita S. Lucia sopra Contesse 5, 98126 Messina, Italy;

* Correspondence: Correspondence: lofaro@itae.cnr.it; Tel.: +39-090624243

Abstract: The co-electrolysis of CO_2 and H_2O at intermediate temperature is a viable approach for the power-to-gas conversion that deserves for further investigation, considering the need for green energy storage. The commercial solid oxide electrolyser is a promising device, but it is still facing to solve issues concerning the high operating temperatures and the improvement of gas value. In this paper we reported the recent findings of a simple approach that we have amply suggested for solid oxide cells consisting in the addition of a functional layer coated to the fuel electrode of commercial electrochemical cells. This approach simplifies the transition to the next generation of cells manufactured with the most promising materials currently developed and improves the gas value in the outlet stream of cell. Here, the material in use as a coating layer consisted of a Ni-modified $La_{0.6}Sr_{0.4}Fe_{0.8}Co_{0.2}O_3$ which was developed and demonstrated as promising fuel electrode for solid oxide fuel cells. The results discussed in this paper proved the positive role of Ni-modified perovskite as a coating layer for the cathode, since an improvement of about twice was obtained about the quality of gas produced.

Keywords: Valorization of CO_2; Solid Oxide Electrochemical Cells; Green methane; Energy storage; Power-to-gas

1. Introduction

The most advanced countries are currently facing environmental threats rising from the climate-changing emissions. Their actions are addressed to a rational use of energy, adopting a circular economy, and acting on the environmental restoring [1-3]. In this context, the theme of song "what goes around comes around" sounds more than ever as an action point for societies, policy makers, and scientists[4]. For what concerns with the research, one possible action is the capture, reuse and valorisation of CO_2 produced by many industrial sectors and the following production of fuels [5]. If this action is coupled with the need to the storage of renewable electricity, the derived fuels belong to a sustainable vision and fully flagged as "green"[6]. A possible way to achieve this target is the use of solid oxide electrochemical cells (SOECs) based technology, which have been used for the conversion of H_2O and CO_2 in syngas at high temperatures [7-9]. Currently, commercial SOECs are manufactured with the same materials and architecture of solid oxide fuel cells (SOFCs) simply because of their robustness [10-14]. However, the use of metallic Ni combined with yttria-stabilized zirconia (YSZ) as fuel electrode (cathode) has an imply on the quality of the outlet gas. In practise, under conventional operating conditions, the fuel in the outlet gas stream is constituted only of H_2 and CO [15-18]. Furthermore, SOECs fed with CO_2 and H_2O were operated at high temperatures (above 800 °C) to minimise the effect of carbon deposition on Ni [19, 20]. But, the high temperatures promote the agglomeration of Ni [21, 22] and suppress the presence of methane as it is thermodynamically stable only at lower temperatures [23, 24]. The commercial approach used to increase the value of syngas and to decrease the intrinsic risk of CO injection in the gas pipeline

 doi:10.20944/preprints202012.0565.v1

consists on the use of a post chemical processor operating in the range of temperatures between 200 °C and 400 °C [25-27]. This approach is exactly the same as the combination of a SOFC with an external reformer and implies an increase in complexity and risks for the overall system [28-31]. An emerging option to improve the chemical reactions occurring on both SOECs and SOFCs cells consists on the addition of a functional layer coated on the fuel electrode. This option is beneficial for the overall system since the dimension and management of system are simplified. Furthermore, the addition of a coating layer on the fuel electrode does not imply any strong change in the manufacturing chain of cells and stacks. The use of cermets (i.e. a combination between metallic and ceramic phases) is the preferred approach owing to the physico-chemical compatibility between these materials and the fuel electrode of solid oxide cells (SOCs) [32-34] .

Based on these results achieved with SOFCs, the authors have suggested a similar approach for the SOECs to enhance the methane production. In 2020, two studies published on "Journal of Energy Storage" [35] and on "International Journal of Hydrogen Energy" [36] reported on the findings of Ni-Fe and Cu-Sn alloys combined with CGO as possible functional layers for commercial SOC cells. By comparing gas chromatographic analyses of the outlet gas of these two cells and of a bare cell, it was found that the quality of outlet gas can be improved by operating intermediate temperatures and though the simply addition of a functional layer to a commercial SOEC cell.

But, a new class of materials corresponding to “exsolved perovskite” has been recently used as fuel electrode for SOC cells [37-43]. These materials have a unique morphology based on a substrate having mixed ionic and electronic conductivity (MIEC) supporting encapsulated fine particles that originate from the segregation of metals from the MIEC's bulk [44, 45]. As a consequence of this exotic structure, these materials show bi-functional properties (i.e. catalytic and electrocatalytic properties) and these are additional to the well-known properties of perovskite towards the resilience to organic-based fuels, redox properties, resistance to sulphur contaminations [46]. Above all, the Ni-modified $La_{0.6}Sr_{0.4}Fe_{0.8}Co_{0.2}O_3$ based perovskite is one of the most known exsolved perovskites under study. Its electrochemical properties were evaluated in a fuel flexible SOFC [47] and in an all-perovskite based SOFC [48]. Here, this paper is devoted to the findings concerning the gas quality of a SOEC cell coated with the Ni-modified $La_{0.6}Sr_{0.4}Fe_{0.8}Co_{0.2}O_3$ based perovskite for the co-electrolysis of H_2O and CO_2. Hence, in this study we reported the preliminary tests conducted by coupling an electrochemical diagnosis of cell and gas outlet analysis. The results are discussed considering our previous achievements with a bare cell investigated under same conditions [49, 50].

2. Results and discussion

The electrochemical tests were carried out for 80 h in a range of temperatures between 525 - 800 °C and by moving the cell between the open circuit voltage and operation condition at 150 mA cm^{-2}. To achieve a stable condition, we kept the cell in each condition for the minimum of 5 h since the GC analysis of effluent gas required 10 min and the measures were repeated 5 times. In some case we kept the cell for more time according to the night rests. At the end point of each thermal and current conditions, polarization curve (current-potential, I-V) and impedance spectroscopy at OCV and at 1.3 V (EIS) have returned information about the behaviour of cell in terms of any possible activation, ohmic and diffusive constraints, the effect of temperature on the OCV and on the kinetic of reactions, etc. Such tests were reported in the supplementary materials since this paper was mainly devoted to the discussion of GC results and on the finding of the most promising operating conditions. This range of temperatures and the current density circulated in the cell under operating conditions were selected according to the characteristic of cell. Below the lower temperature investigated (i.e. 525 °C), too high constraints derived from the ohmic resistance of the electrolyte and from the overpotential due to the evolution of oxygen (i.e. reaction occurring at the anode of cell) did not permit a circulation of an adequate current. At 525 °C, the maximum current density permitted was 150 mA cm^{-2}. Above this value, a voltage higher than 2 V was recorded and this value did not comply with the efficient use of this technology and with the risk of cell and housing degradation. However, this value of current is still acceptable since it is close to the practical long-term operating condition of commercial cells. Temperatures over 800 °C were not investigated since they are not requested from technology

Preprints (www.preprints.org) | NOT PEER-REVIEWED | Posted: 22 December 2020 doi:10.20944/preprints202012.0565.v1

challenges and utilisation and as a consequence these temperatures, in principle, should be avoided. In addition, the commercial cell selected for this experiment was optimised for operation at intermediate temperature. In fact, the ASC-400B of Elcogen possess a double thin electrolyte (lower than 5 μm together) and a pure cobaltite as an anode, which is currently considered the most performant oxygen electrode. Nevertheless, ASC-400B cells are optimised for SOFC operation and are simply adapted to SOEC operation. But, a relapse of this adaptation consists on an anode-electrolyte interface morphology not fully optimised for high current density. It is largely reported in the literature about the high risks of delamination occurring at the anode-electrolyte interface where high flow of molecular oxygen (occurring at high current density) literally "bubbling" during its evolution at the anode side [51, 52]. Based on these considerations, a fixed current density of 150 mA cm^{-2} has been adopted for the tests.

Figure 1 depicts the overall operation time for the cell. We observe that both OCV and cell voltage at 150 mA cm^{-2} were strongly affected by the increased temperature. As observed, the cell operates above the thermoneutral potential only at 525 °C, whereas from 550 °C the cell operated at a voltage below the thermoneutral potential. [53]. The decrease of OCV with increased temperatures is a consequence of the reversible potential due to H_2/O_2 reaction. Instead, the decrease in cell voltage at 150 mA cm^{-2} is due to the positive effects of increased temperature on both activation and ohmic constraints as it was also proved from the EIS and I-V tests reported in the SI. Furthermore, the OCV recorded up to 700 °C was close to 1 V as a prove of limited or none gas leakages from the cathode chamber. Nevertheless, at higher temperatures, a significantly increased noise and relevant cell voltage loss suggested a chemical degradation of cell due to increased kinetics for the re-oxidation of Ni as a consequence of the low amount of H_2 and of the presence of H_2O and CO_2 fed to the cathode (eqs. 1–2). However, the re-oxidation of Ni as a consequence of possible leakage of O_2 from the atmospheric air is negligible because the high OCV recorded (fig. 1) and because the carbon balance was close to 1 at all temperatures investigated (see the supporting information).

$$Ni + H_2O \rightarrow NiO + H_2 \quad (1)$$

$$Ni + CO_2 \rightarrow NiO + CO \quad (2)$$

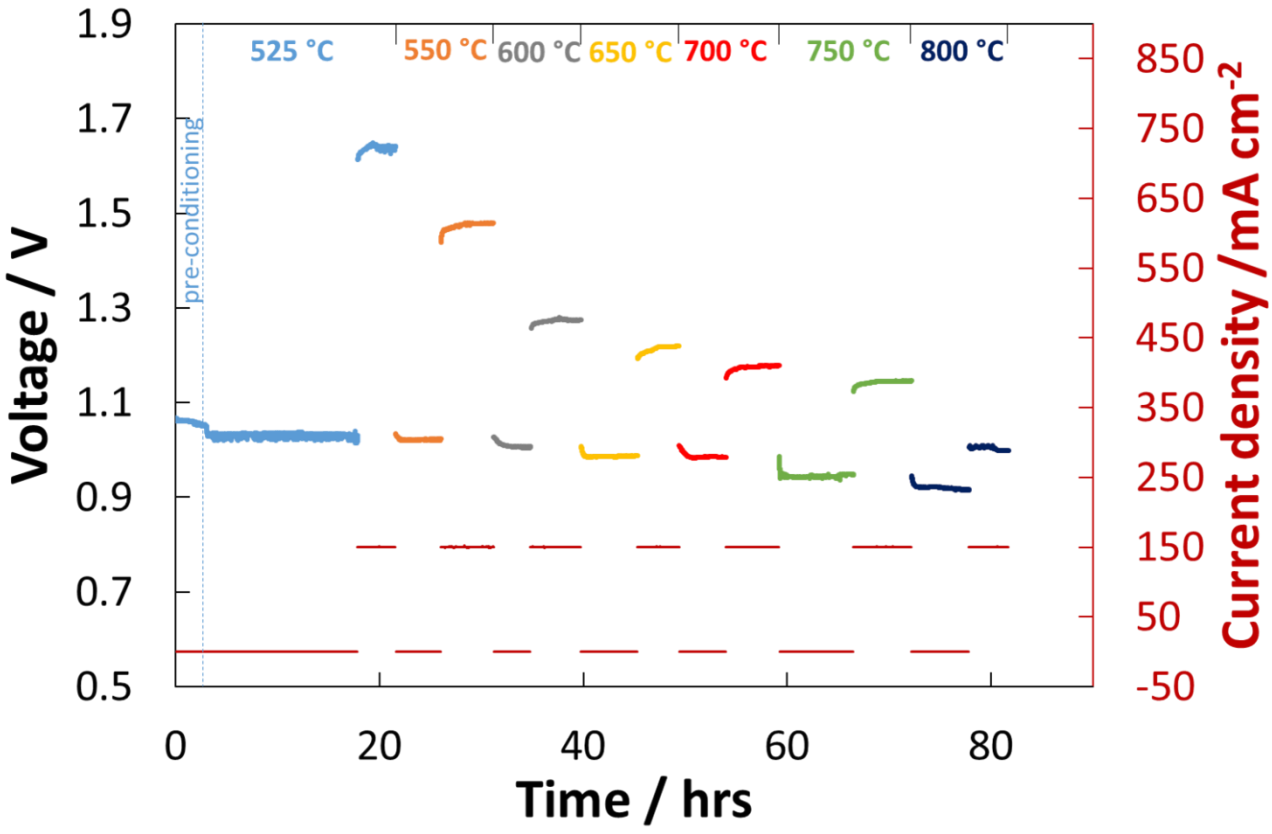

Preprints (www.preprints.org) | NOT PEER-REVIEWED | Posted: 22 December 2020 doi:10.20944/preprints202012.0565.v1

Figure 1. Life–time test for the coated cell investigated in the temperature range 525–800 °C Figure 2. O and CO_2.

In the Table 1 were reported the main electrochemical results achieved for the bare and coated cells. It is worthy as the coated cell showed significantly lower performance, especially at intermediate temperatures. Such behaviour is a direct consequence of limited conductivity of perovskite compared to Ni-YSZ, as it is proved from the differences of Area Specific Resistance (ASR) values reported in table 1.

Table 1. Most relevant electrochemical results achieved with bare and coated cells.

		Temperature						
		525 °C	**550 °C**	**600 °C**	**650 °C**	**700 °C**	**750 °C**	**800 °C**
Cell Voltage at 150 mA cm^{-2}	***Coated cell***	1.88 V	1.48 V	1.24 V	1.24 V	1.24 V	1.11 V	1.00 V
	Bare cell [ref. 50]	1.15 V	1.07 V	0.99 V	0.94 V	0.91	n.a.	n.a.
Area Specific Resistance at 150 mA cm^{-2}	***Coated cell***	>16 Ω cm^2	3.51 Ω cm^2	2.07 Ω cm^2	1.80 Ω cm^2	1.72 Ω cm^2	1.33 Ω cm^2	0.69 Ω cm^2
	Bare cell [ref. 50]	2.89 Ω cm^2	2.25 Ω cm^2	1.24 Ω cm^2	0.81 Ω cm^2	0.76 Ω cm^2	n.a.	n.a.

The results of gas-chromatographic experiments were treated according to the following equations:

$$CO_2\ conversion\ (\%) = \frac{CO_{2_{in}} - CO_{2_{out}}}{CO_{2_{in}}} \quad (3)$$

$$H_2\ residue\ (\%) = \frac{H_{2_{out}}}{H_{2_{in}}} \quad (4)$$

$$Selectivity\ to\ CO\ (\%) = \frac{CO_{out}}{CO_{2_{in}}} \quad (5)$$

$$CO\ yield\ (\%) = CO_2\ conversion * CO\ selectivity \quad (6)$$

$$Selectivity\ to\ CH_4(\%) = \frac{CH_{4_{out}}}{CO_{2_{in}}} \quad (7)$$

$$CH_4\ yield\ (\%) = CO_2\ conversion * CH_4\ selectivity \quad (8)$$

These results were compared with theoretical data at OCV (i.e. without the ionic oxygen moved from the cathode to the anode through the electrolyte) obtained using the GASEQ software.

The experimental data treated accordingly to equation 3 and the simulated data for similar conditions are reported in figure 2. Chemical (eqs. 2, 9-11) and electrochemical reactions (eqs. 12–14) were involved in the CO_2 conversion. An error bar related to systematic errors occurring during GC analysis was added. In this figure, it is worthy to note the low reactivity of CO_2 and a sensible deviation from the thermodynamic values, especially at lower temperatures. Nevertheless, the circulation of current has increased the conversion of CO_2 as a consequence of the simultaneous occurrence of its electrochemical (eq. 12) and chemical (eq. 9) reduction. In principle, the high temperatures and the increased partial pressure of H_2 produced from the electrochemical reduction of H_2O (eq. 15) moved the chemical reduction of CO_2 to CO (eq. 9). In addition, a significant increase in this trend was observed at temperatures above 700 °C as a consequence of the increased kinetic involving the CO_2 with Ni to form NiO (eq. 2).

$$CO_2 + H_2 \rightarrow CO + H_2O \quad (9)$$

Preprints (www.preprints.org) | NOT PEER-REVIEWED | Posted: 22 December 2020 doi:10.20944/preprints202012.0565.v1

$$CO_2 + 2H_2 \rightarrow C + 2H_2O \quad (10)$$

$$CO_2 + 4H_2 \rightarrow CH_4 + 2H_2O \quad (11)$$

$$CO_2 + 2e^- \rightarrow CO + O^{2-} \quad (12)$$

$$CO_2 + 4e^- \rightarrow C + 2O^{2-} \quad (13)$$

$$CO_2 + 2H_2O + 8e^- \rightarrow CH_4 + 4O^{2-} \quad (14)$$

These results were similar to that achieved with the bare cell up to 650°C and proves that the functional layer was not extremely active at intermediate temperatures (table 2). A significant increase is instead observed at temperatures above 700 °C as a clear evidence of the role played from the functional layer.

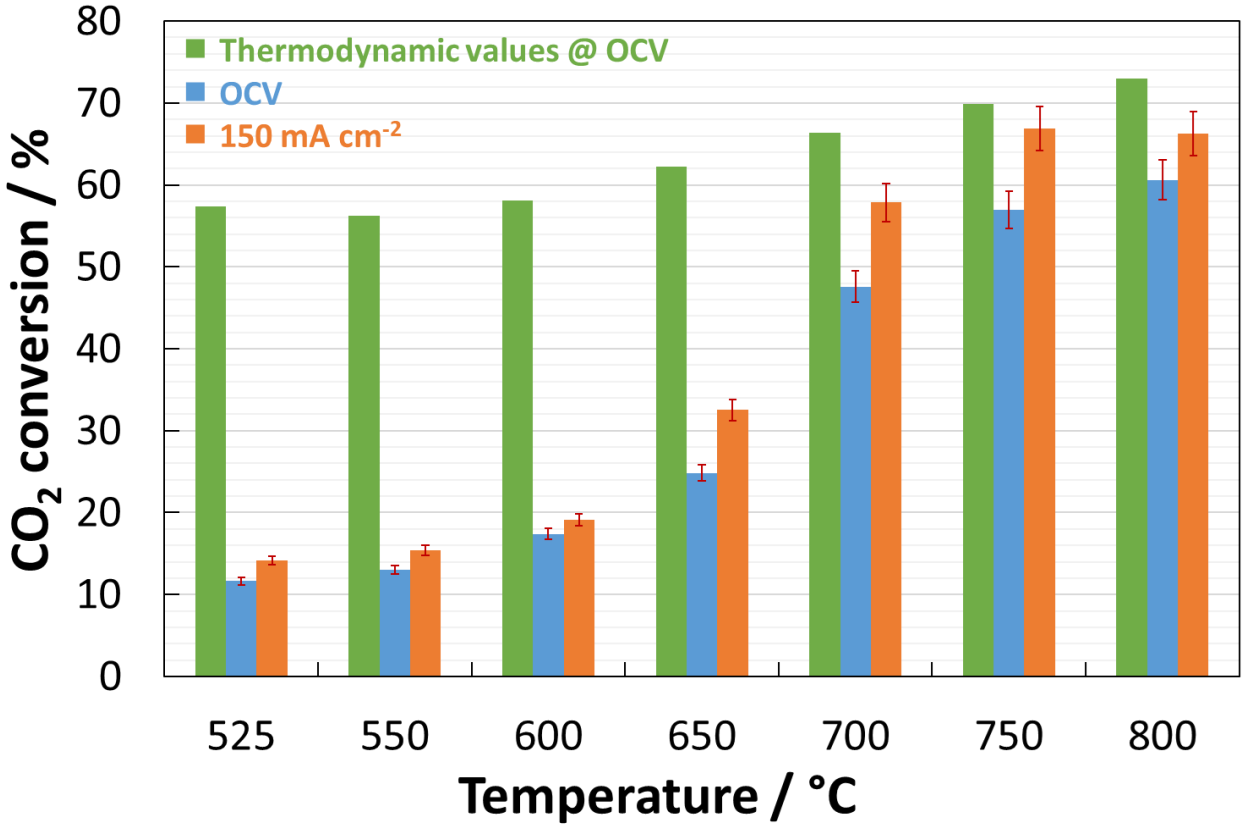

Figure 2. CO_2 conversion based on thermodynamic prediction and under practical conditions treated accordingly to equation 3 .

The evaluation of H_2 content in the outlet gas is presented in figure 3, where the comparison of results achieved in two practical conditions (i.e. OCV and 150 mA cm^{-2}) and the data predicted thermodynamically is reported. Under the circulation of current, the reduction of H_2O is expected:

$$H_2O + 2e^- \rightarrow H_2 + O^= \quad (15)$$

This figure shows two important aspects of experimental results. The first concerns with the deviations at low temperatures between the bar charts under practical conditions and thermodynamic values that are mainly due to limited CO_2 chemical reduction as observed in figure 2. The second aspect is related to the H_2 residue less than 100 % under practical conditions (compared to the inlet) and this means that H_2 is consumed from the reduction of CO_2 and CO, and to maintain Ni under metallic state. These reactions are temperature-activated and justify the trends observed for the conversion of CO_2 (fig. 1). Also, the contrary trends observed for the thermodynamic and practical conditions bar charts are an evidence of H_2 demand due to the parasitic reactions occurring under practical conditions and involving the Ni. Here, the behaviour of this cell was similar to that of bare

Preprints (www.preprints.org) | NOT PEER-REVIEWED | Posted: 22 December 2020 doi:10.20944/preprints202012.0565.v1

cell, demonstrating a limited promoting role of the functional layer towards the reduction of H_2O (table 2).

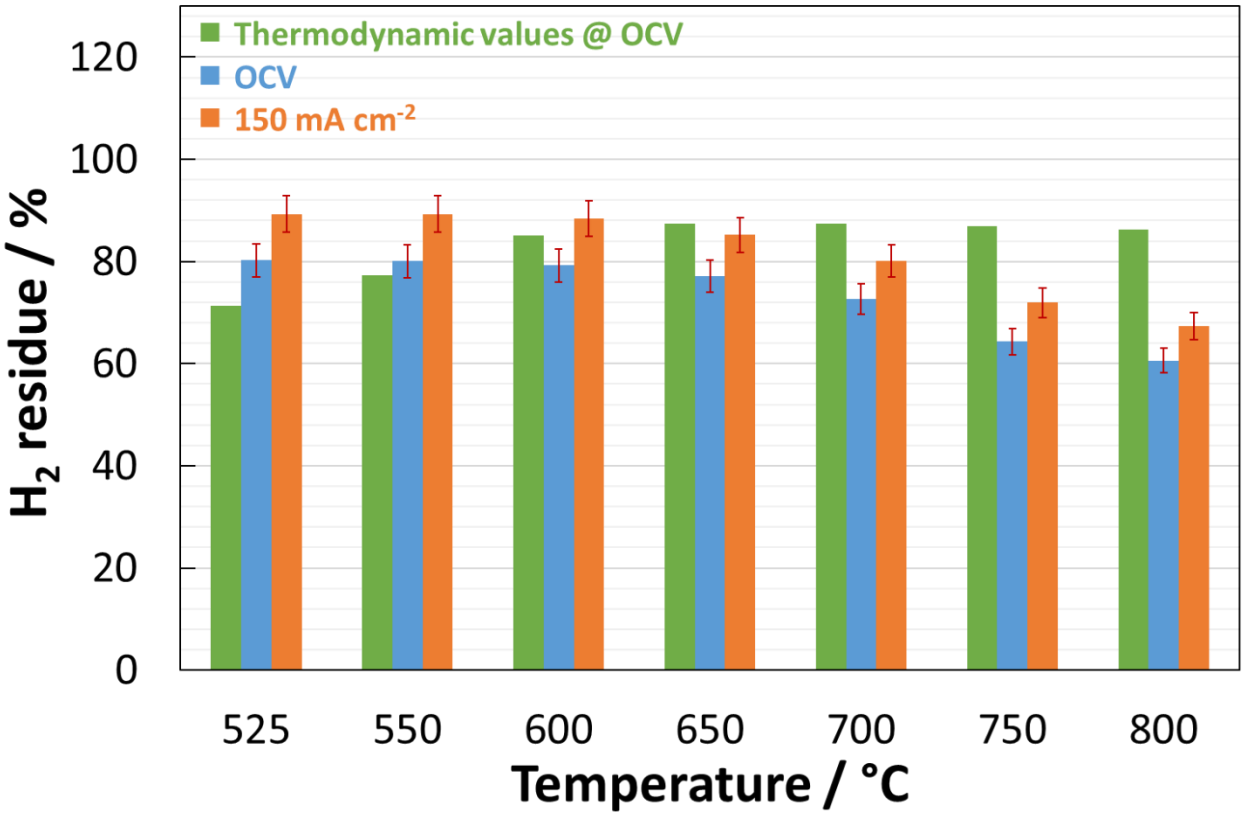

Figure 3. Trend of H_2 residue based on thermodynamic prediction and under practical conditions treated accordingly to equation 4 .

The data related to CO residue were treated according to equations 5 and 6. The figure 4a depicts the trend for selectivity to CO in the temperature range of 525 – 800 °C. As shown, the cell promoted a high selectivity to CO as expected from its favourable thermodynamic formation with increasing temperatures. At 525 °C the selectivity to CO was approximately 95 % under OCV and 92 % under the circulation of current and higher than expected on the basis of thermodynamic results. By increasing the temperature, these values increased too and reached 100 % at 650°C. However, one positive aspect was that the circulation of the current slightly depleted the selectivity to CO. Such behaviour was evident at 525°C and indicates a minor contribution of equation 12 to the overall conversion of CO_2.

The figure 4b reports the CO yield evaluated according to equation 6. The trends of bar charts for the experimental data were in agreement with the thermodynamic data. Nevertheless, the yield of CO observed in the outlet gas was significantly lower than the predicted yield as a consequence of low reactivity of CO_2, as discussed for figure 2. Furthermore, the positive effect on the CO yield observed for the study case with a current density of 150 mA cm^{-2} was a consequence of the increased H_2 partial pressure on the reaction 9 produced from the direct conversion of H_2O (eq. 15).

Preprints (www.preprints.org) | NOT PEER-REVIEWED | Posted: 22 December 2020 doi:10.20944/preprints202012.0565.v1

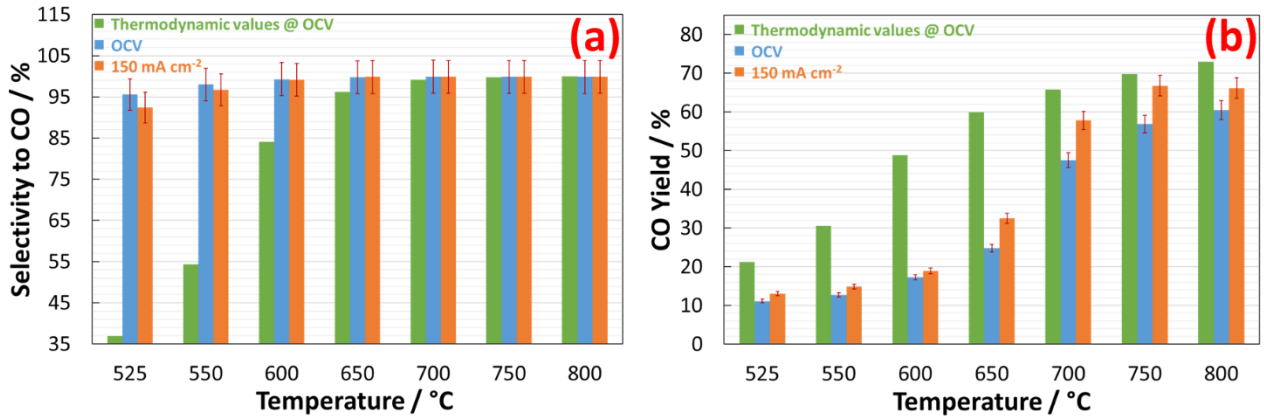

Figure 4. Trend of CO selectivity (a) and yield (b) treated accordingly to equations 5 and 6 .

Concerning the CH_4 residue in the outlet gas, the data were treated accordingly to equations 7 and 8. The Fig. 5a shows that the selectivity to CH_4 is relatively low and limited to the intermediate temperatures. This behaviour is in agreement with the thermodynamic trend for methane stability, which requests for temperatures below 650 °C to become favourable compared to CO. Nevertheless, the circulation of the current in the cell at 525 °C promoted a significant increase in selectivity to methane. Although this behaviour can be ascribed to the direct methanation of CO_2 (eq. 14), the low electrochemical reactivity of CO_2 (see fig. 2) suggests that the CH_4 was produced through the combination of CO_2 and H_2. As discussed for the production of CO (fig. 3) a consequence of the increased H_2 partial pressure promoted by the electrochemical reduction of H_2O (eq. 19) can affect the quality of the outlet gas. However, the CH_4 yield (fig. 5b) measured during the cell operation was significantly lower to the predicted values and it is the direct consequence of low reactivity of CO_2 towards its catalytic and electrocatalytic reduction.

In terms of trends, the bar charts reported for the CO (fig. 4) and CH_4 (fig.5) were similar to that achieved for a bare cell. Nevertheless, by comparing the absolute values recorded in these two experiments, it was proved as the addition of Ni-modified LSFCO increased the quality of outlet gas of about twice in terms of CH_4 yield (table 2).

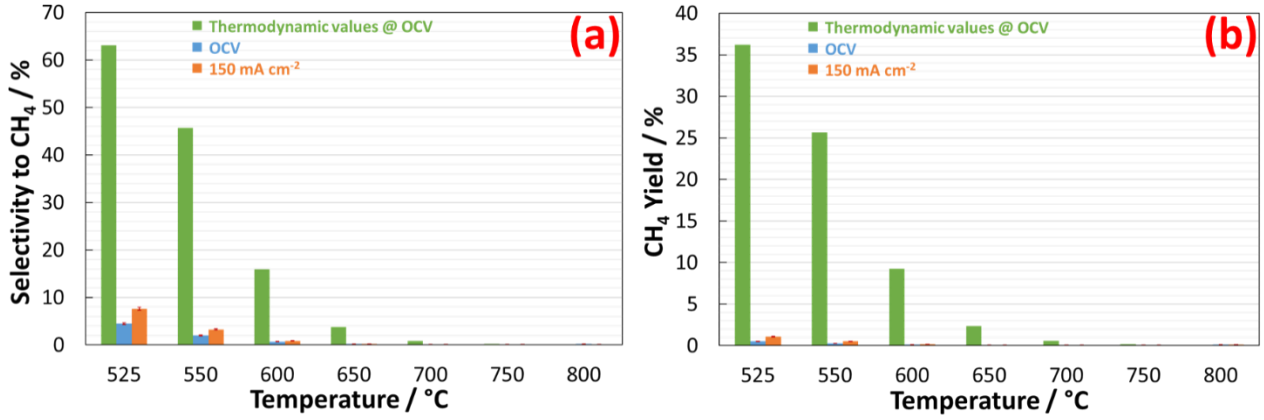

Figure 5. Trend of CH_4 selectivity (a) and yield (b) treated accordingly to equations 7 and 8 .

In table 2 are summarized the results of gas-chromatographic tests concerning bare and coated cells under the current density of 150 mA cm^{-2}. As discussed, the addition of coating layer to the bare cell was not particularly effective for a significant increase in CO_2 and H_2O conversion at temperatures below 600 °C, although at higher temperatures the promoting effect of perovskite was observed. Nevertheless, it is sensible as the coating layer has promoted an increased quality of gas as a consequence of reduced amount of CO and increased amount of CH_4.

Preprints (www.preprints.org) | NOT PEER-REVIEWED | Posted: 22 December 2020 doi:10.20944/preprints202012.0565.v1

Table 2. Most relevant chromatographic data achieved with bare and coated cells.

		Temperature						
		525 °C	**550 °C**	**600 °C**	**650 °C**	**700 °C**	**750 °C**	**800 °C**
Coated cell -@ 150 mA cm^{-2}-	***CO_2 conversion***	14.1 %	15.4 %	19.1 %	32.5 %	57.9 %	66.8 %	66.3 %
	H_2 residue	89.2 %	89.2 %	88.4 %	85.2 %	80.11 %	71.9 %	67.4 %
	Selectivity to CO	92.4 %	96.7 %	99.1 %	99.8 %	99.9 %	99.9 %	99.8 %
	CO yield	13.1 %	14.9 %	19.0 %	32.5 %	57.8 %	66.8 %	66.1 %
	Selectivity to CH_4	7.6 %	3.2 %	0.8 %	0.2 %	0.1 %	0.1 %	0.2 %
	CH_4 yield	1.1 %	0.5 %	0.2 %	0.1 %	0.1 %	0.1 %	0.1 %
Bare cell -@ 150 mA cm^{-2}- *[ref. 50]*	***CO_2 conversion***	25.9 %	26.9 %	29.8 %	30.3 %	31 %	n.a.	n.a.
	H_2 residue	107 %	108.1 %	108.2 %	103.7 %	98.9 %	n.a.	n.a.
	Selectivity to CO	97.9 %	99.2 %	99.9 %	100 %	100 %	n.a.	n.a.
	CO yield	25.4 %	26.7 %	29.7 %	30.3 %	30.9 %	n.a.	n.a.
	Selectivity to CH_4	2.1 %	0.8 %	0.1 %	0 %	0 %	n.a.	n.a.
	CH_4 yield	0.5 %	0.2 %	traces	traces	traces	n.a.	n.a.

Concerning the possible formation of carbon as a consequence of the chemical (eq. 10) and electrochemical (eq. 13) reactions, the sum of C species determined in the gas effluent was closed to 100 % (see the SI).

An indication on the efficiency of chemical and electrochemical reactions related to the production of CO and CH_4 is given through the treatment of gas-chromatographic data according to the following equations:

$$\xi_{CO_{chem}}(a.u) = \frac{total\ CO\ produced}{H_2\ inlet} \quad (16)$$

$$\xi_{CH_{4\,chem}}(a.u) = \frac{total\ CH_4\ produced}{4H_2\ inlet} \quad (17)$$

$$\xi_{CO_{Faradaic}}(a.u.) = \frac{total\ CO\ produced}{CO\ electrochem\ obtainable} \quad (18)$$

$$\xi_{CH_{4Faradaic}}(a.u.) = \frac{total\ CH_4\ produced}{CH_4\ electrochem\ obtainable} \quad (19)$$

where $CO_{electrochem\ obtainable}$ and $CH_{4_{electrochem\ obtainable}}$ are derived according to the following equations:

$$CO_{electrochem\ obtainable}({}^{cc}/_{\min\ cm^2}) = \frac{current\ density}{n\ \cdot F} \quad (20)$$

$$CH_{4_{electrochem\ obtainable}}({}^{cc}/_{\min\ cm^2}) = \frac{current\ density}{n\ \cdot F} \quad (21)$$

Preprints (www.preprints.org) | NOT PEER-REVIEWED | Posted: 22 December 2020 doi:10.20944/preprints202012.0565.v1

The current density circulated into the cell was 150 mA cm^{-2}. The term "n" is the number of electrons involved in the reducing reaction of CO_2. In the case of CO, n is equal 2, according to eq. 16, whereas in the case of CH_4, n is equal to 8 according to equation 18. F is the Faradaic constant.

The $\xi_{X_{chem}}$ provides an indication of how effective is the chemical reaction producing the X species and $\xi_{X_{Faradaic}}$ is estimated on the basis of theoretically electrochemical production of X species. Values $\xi > 1$ are possible only if the electrochemical reduction of CO_2 adds to the CO or CH_4 formation. In the contrary case, the electrochemical conversion of CO_2 is less probable but cannot be excluded.

The bar charts reported in the figure 6a represent the efficiency to CO formation (eqs. 16 and 18) expressed in arbitrary units (a.u.). As shown, the data at OCV are close to the thermodynamic values but, circulation current in the cell, a great enhancement in the efficiency of CO yield was observed. At 150 mA cm^{-2}, the electrochemical reduction of both CO_2 (eq. 12) and H_2O (eq. 15) is expected, although, as discussed above, the first reaction is limited, especially at lower temperatures. As consequence, the bar charts at 150 mA cm^{-2} at lower temperature are enhanced due to the reverse water-gas shift reaction (eq. 9) whereas, starting from 650 °C the direct electrochemical conversion of CO_2 to CO becomes dominant (eq. 12) since ξ was higher than 1. A similar treatment of data was developed for the evaluation of efficiency to methane production according to eqs. 17 and 19. As depicted in the figure 6b, the methane produced by a pure chemical reaction is negligible as also the thermodynamics predicts. CH_4 is in-fact largely unstable at temperatures and many parallel reactions (including cracking) concur with its low presence at the outlet. Under the circulation of the current, the concurrent multiple electrochemical reduction of both CO_2 to CO (eq. 10) and to C (eq. 11) along with the high partial pressure of H_2 produced electrochemically cooperate to the formation of methane with an efficiency higher than the predicted.

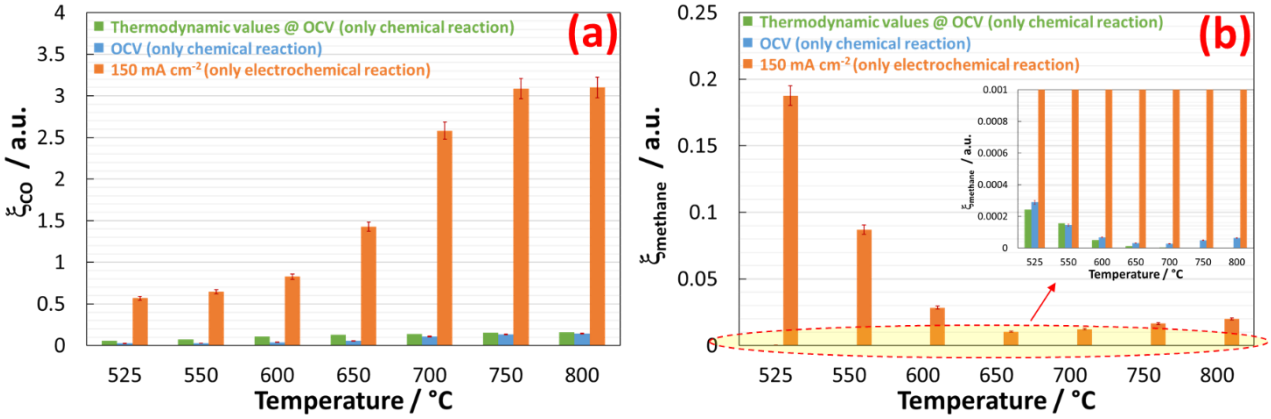

Figure 6. Trend of efficiency towards the production of CO (a) and methane (b) determined using equations 16 –19.

3. Experimental

The exsolved perovskite used as functional layer is referred to as Ni-modified $La_{0.6}Sr_{0.4}Fe_{0.8}Co_{0.2}O_3$ (LSFCO). The procedure used is referred to the wet impregnation of LSFCO (Praxair) with 3 wt. % of Ni (Ni as nitrate, Sigma Aldrich). After drying, the impregnated powders were calcined for 2 h at 500 °C in air and then reduced for 2 h at 800 °C with dilute H_2 (5 vol. %). As a result of thermal treatments, a partial segregation of Fe and Co from the bulk of perovskite moved to the surface and combined with Ni to form fine embedded nanoparticles on the surface of the depleted LSFCO. The resulting phases were a Ruddlesden–Popper-type structure and a solid oxide solution between Ni, Fe, and Co (i.e. α-$Fe_{100-y-z}Co_yNi_zO_x$ oxide). This exotic material was extensively investigated from the authors of this work and reported in other papers. The functional layer used for this research consisted of a ball-milled mixture of 70 wt. % of Ni-modified perovskite and 30 wt. % of CGO (Sigma Aldrich). Then, the cathode of the SOEC cell was brush coated with a slurry of the functional layer including 3 wt.% of Butvar (Sigma Aldrich) and 1 wt.% α-terpineol (Sigma Aldrich)

 doi:10.20944/preprints202012.0565.v1

and ethanol as solvent in an amount of at least 60 wt. %. The cell used for this experiment was a button cell with an active area of 2 cm^2 cut from a large planar cell manufactured by Elcogen. This cell is referred to ASC-400B and consists of a Ni-YSZ cathode, YSZ and CGO double electrolytes and $La_{0.6}Sr_{0.4}CoO_3$ (LSC) anode. A pre-conditioning step of 2 h carried out at 800 °C in presence of diluted gas was carried out to promote the exsolution of perovskite and its adhesion with the cathode of the cell. Then, the cell was cooled to up 525 °C and the gas inlet was set to H_2 (2.5 cc min^{-1} cm^{-2}), He (15 cc min^{-1} cm^{-2}), H_2O (fed by a syringe pump at 0.005 g h^{-1} cm^{-2} and then vaporized), and CO_2 (1 cc min^{-1} cm^{-2}) at the cathode and Air (50 cc min^{-1} cm^{-2}) at the anode. The cell was experimented in a test bench purchased from the Greenlight Innovation company. The electrochemical characterization of cell was carried out with a BioLogic instrument and the dried effluent gas from the cathode analysed by a micro-(VARIAN) equipped with Molsieve (20 mt), PoraPLOT Q (10 mt), CB-Sil (8 mt) and micro-DMD (Differential Mobility Detector). The GC results were treated according to a prior calibration carried out with gas calibration mixes purchased from Sigma Aldrich.

4. Conclusions

Ni-modified $La_{0.6}Sr_{0.4}Fe_{0.8}Co_{0.2}O_3$ was deeply investigated as an anode for SOFC and can also be suggested as a cathode for SOECs because of redox behaviour of perovskite and because commercial cells based on Ni-based cathode have a high risk of cracking as a consequence of an extensive redox cycle when H_2O is fed to the cell [54]. In this work, we report the study of a commercial SOEC coated on the cathode with a functional layer based on this material that was reported in the literature to be exsolved under reducing conditions and effective for the tuning of the outlet gas quality during the co-electrolysis of CO_2 and H_2O [55]. The experiments conducted in the range of temperature between 525 – 800 °C showed the behaviour of the cell in terms of electrochemical characteristics and gas stream quality from the cathode chamber. The electrochemical behaviour of cell showed that the addition of a functional layer negatively affected the voltage of the cell as a consequence of limited conductivity of perovskite. Furthermore, we discussed the role of Ni-modified perovskite in the gas quality produced during the electrochemical conversion of CO_2 and H_2O. The treated data concerning the outlet gas stream were discussed in relation of our recent achievements concerning a bare cell investigated under same conditions. As discussed in this paper, the use of a Ni-modified perovskite reduced the reactivity of CO_2, especially at temperatures below 650 °C where the preferred reaction was the electroreduction of H_2O. However, the most significant achievement consisted of the increased gas quality in terms of increased yield of methane and depletion of CO at intermediate temperatures of at least twice compared to the bare cell. Therefore, the results proved that an optimised exsolved perovskite used as a coating layer for a SOEC is an effective approach for the progress of SOEC technology towards the co-electrolysis of H_2O and CO_2.

Author Contributions: Conceptualization, A.S.A. and M.L.F.; methodology, A.S.A. and S.C.Z.; software, M.L.F.; analysis, S.C.Z. and M.L.F.; investigation, S.C.Z.; writing—original draft preparation, M.L.F. and A.S.A.; writing—review and editing, M.L.F. and A.S.A.; project administration, A.S.A.; funding acquisition, V.A.. All authors have read and agreed to the published version of the manuscript.

Funding: The present work was carried out within an Agreement between the Italian Ministry of Economic Development (MISE) and the National Research Council (CNR) in the framework of a Research Program for the Electric System (RdS-PAR2019).

Abbreviations

Acronym	Full form
ASC	Anode Supporting Cell
ASR	Area Specific Resistance
a.u.	arbitrary unit

 doi:10.20944/preprints202012.0565.v1

CGO	$Ce_{0.9}Gd_{0.1}O_{2-\delta}$
GC	Gas-Chromatography
GDC	Gadolinia-Doped Ceria
LSC	$La_{0.6}Sr_{0.4}CoO_3$
LSFCO	$La_{0.6}Sr_{0.4}Fe_{0.8}Co_{0.2}O_3$
MIEC	Mixed Ionic and Electronic Conductor
n.a.	data not available
OCV	Open Circuit Voltage
SOEC	Solid Oxide Electrolysis Cell
SOFC	Solid Oxide Fuel Cell
SOC	Solid Oxide Cell
YSZ	Yttria-stabilized Zirconia

References

1. [1] R.D. Marchand: S.C.L.; Koh, J.C.; Morris, Delivering energy efficiency and carbon reduction schemes in England: Lessons from Green Deal Pioneer Places, Energy Policy, 84 (2015) 96-106.
2. [2] H.; Pettifor, C. Wilson, G. Chryssochoidis, The appeal of the green deal: Empirical evidence for the influence of energy efficiency policy on renovating homeowners, Energy Policy, 79 (2015) 161-176.
3. [3] A. Sikora, European Green Deal – legal and financial challenges of the climate change, ERA Forum, (2020).
4. [4] K.J. Lau, P.I. Tokofsky, S.D. Winick, What goes around comes around: The circulation of proverbs in contemporary life, What Goes Around Comes Around2004, pp. 1-19.
5. [5] E.I. Koytsoumpa, C. Bergins, E. Kakaras, The CO2 economy: Review of CO2 capture and reuse technologies, Journal of Supercritical Fluids, 132 (2018) 3-16.
6. [6] G. Centi, S. Perathoner, Green Carbon Dioxide: Advances in CO2 Utilization, 2014.
7. [7] C. Graves, S.D. Ebbesen, M. Mogensen, K.S. Lackner, Sustainable hydrocarbon fuels by recycling CO2 and H2O with renewable or nuclear energy, Renewable and Sustainable Energy Reviews, 15 (2011) 1-23.
8. [8] E. Ioannidou, S. Neophytides, D.K. Niakolas, Experimental Clarification of the RWGS Reaction Effect in H2O/CO2 SOEC Co-Electrolysis Conditions, Catalysts, 9 (2019) 151.
9. [9] M. Guo, X. Ru, Z. Lin, G. Xiao, J. Wang, Optimization Design of Rib Width and Performance Analysis of Solid Oxide Electrolysis Cell, Energies, 13 (2020) 5468.
10. [10] A. Glauche, T. Betz, M. Ise, Product development for SOFC and SOE applications, ECS Transactions, 2011, pp. 157-165.
11. [11] A. Aguilo-Rullan, M. Atanasiu, B. Biebuyck, N. Lymperopoulos, C. Marenco, D. Tsimis, The status of SOFC and SOEC R&D in the European fuel cell and hydrogen joint undertaking programme, ECS Transactions, 2017, pp. 41-61.
12. [12] R. Küngas, P. Blennow, T. Heiredal-Clausen, T.H. Nørby, J. Rass-Hansen, S. Primdahl, J.B. Hansen, ECOs - A commercial CO2 electrolysis system developed by Haldor Topsoe, ECS Transactions, 2017, pp. 2879-2884.
13. [13] D. Tsimis, A. Aguilo-Rullan, M. Atanasiu, E. Zafeiratou, D. Dirmiki, The status of SOFC and SOEC R&D in the European fuel cell and hydrogen joint undertaking programme, ECS Transactions, 2019, pp. 9-26.

14. [14] R. Küngas, P. Blennow, T. Heiredal-Clausen, T. Holt Nørby, J. Rass-Hansen, J.B. Hansen, P.G. Moses, Progress in SOEC development activities at Haldor Topsøe, ECS Transactions, 2019, pp. 215-223.
15. [15] Y. Redissi, C. Bouallou, Valorization of carbon dioxide by co-electrolysis of CO2/H2O at high temperature for syngas production, Energy Procedia, 2013, pp. 6667-6678.
16. [16] Y. Wang, T. Liu, L. Lei, F. Chen, High temperature solid oxide H2O/CO2 co-electrolysis for syngas production, Fuel Processing Technology, 161 (2017) 248-258.
17. [17] L. Wang, M. Chen, R. Küngas, T.E. Lin, S. Diethelm, F. Maréchal, J. Van herle, Power-to-fuels via solid-oxide electrolyzer: Operating window and techno-economics, Renewable and Sustainable Energy Reviews, 110 (2019) 174-187.
18. [18] J. Kupecki, L. Mastropasqua, K. Motylinski, D. Ferrero, Chapter 5 - Multilevel modeling of solid oxide electrolysis, in: M. Lo Faro (Ed.) Solid Oxide-Based Electrochemical Devices, Academic Press2020, pp. 123-166.
19. [19] M. Navasa, H.L. Frandsen, T.L. Skafte, B. Sundén, C. Graves, Localized carbon deposition in solid oxide electrolysis cells studied by multiphysics modeling, Journal of Power Sources, 394 (2018) 102-113.
20. [20] J. Aicart, F. Usseglio-Viretta, J. Laurencin, M. Petitjean, G. Delette, L. Dessemond, Operating maps of high temperature H2O electrolysis and H2O+CO2 co-electrolysis in solid oxide cells, International Journal of Hydrogen Energy, 41 (2016) 17233-17246.
21. [21] G.J. Nelson, K.N. Grew, J.R. Izzo Jr, J.J. Lombardo, W.M. Harris, A. Faes, A. Hessler-Wyser, J. Van Herle, S. Wang, Y.S. Chu, A.V. Virkar, W.K.S. Chiu, Three-dimensional microstructural changes in the Ni-YSZ solid oxide fuel cell anode during operation, Acta Materialia, 60 (2012) 3491-3500.
22. [22] B. Iwanschitz, L. Holzer, A. Mai, M. Schütze, Nickel agglomeration in solid oxide fuel cells: The influence of temperature, Solid State Ionics, 211 (2012) 69-73.
23. [23] B. Chen, Y.S. Hajimolana, V. Venkataraman, M. Ni, P.V. Aravind, Integration of reversible solid oxide cells with methane synthesis (ReSOC-MS) in grid stabilization: A dynamic investigation, Applied Energy, 250 (2019) 558-567.
24. [24] S. Biswas, A.P. Kulkarni, S. Giddey, S. Bhattacharya, A Review on Synthesis of Methane as a Pathway for Renewable Energy Storage With a Focus on Solid Oxide Electrolytic Cell-Based Processes, Frontiers in Energy Research, 8 (2020).
25. [25] B. Chen, H. Xu, M. Ni, Modelling of SOEC-FT reactor: Pressure effects on methanation process, Applied Energy, 185 (2017) 814-824.
26. [26] E. Giglio, A. Lanzini, M. Santarelli, P. Leone, Synthetic natural gas via integrated high-temperature electrolysis and methanation: Part I-Energy performance, Journal of Energy Storage, 1 (2015) 22-37.
27. [27] P. Frontera, A. Macario, A. Malara, V. Antonucci, V. Modafferi, P.L. Antonucci, Simultaneous methanation of carbon oxides on nickel-iron catalysts supported on ceria-doped gadolinia, Catalysis Today, 357 (2020) 565-572.
28. [28] M. Lo Faro, A. Vita, L. Pino, A.S. Aricò, Performance evaluation of a solid oxide fuel cell coupled to an external biogas tri-reforming process, Fuel Processing Technology, 115 (2013) 238-245.
29. [29] F. Manenti, R. Pelosato, P. Vallevi, A.R. Leon-Garzon, G. Dotelli, A. Vita, M.L. Faro, G. Maggio, L. Pino, A.S. Arico, Biogas-fed solid oxide fuel cell (SOFC) coupled to tri-reforming process: Modelling and simulation, International Journal of Hydrogen Energy, 40 (2015) 14640-14650.
30. [30] M. Lo Faro, S. Trocino, S.C. Zignani, A.S. Aricò, G. Maggio, C. Italiano, C. Fabiano, L. Pino, A. Vita, Study of a Solid Oxide Fuel Cell fed with n-dodecane reformate. Part I: Endurance test, International Journal of Hydrogen Energy, 41 (2016) 5741-5747.
31. [31] M. Lo Faro, S. Trocino, S.C. Zignani, C. Italiano, A. Vita, A.S. Aricò, Study of a solid oxide fuel cell fed with n-dodecane reformate. Part II: Effect of the reformate composition, International Journal of Hydrogen Energy, 42 (2017) 1751-1757.
32. [32] M. Lo Faro, R.M. Reis, G.G.A. Saglietti, A.G. Sato, E.A. Ticianelli, S.C. Zignani, A.S. Aricò, Nickel-Copper/Gadolinium-doped Ceria (CGO) composite electrocatalyst as a protective layer for a Solid-Oxide Fuel Cell anode fed with ethanol, ChemElectroChem, 1 (2014) 1395-1402.
33. [33] M. Lo Faro, R.M. Reis, G.G.A. Saglietti, S.C. Zignani, S. Trocino, P. Frontera, P.L. Antonucci, E.A. Ticianelli, A.S. Aricò, Investigation of Ni-based alloy/CGO electro-catalysts as protective layer for a solid oxide fuel cell anode fed with ethanol, Journal of Applied Electrochemistry, 45 (2015) 647-656.
34. [34] M. Lo Faro, S. Trocino, S.C. Zignani, C. Italiano, R.M. Reis, E.A. Ticianelli, A.S. Aricò, Nickel–Iron/Gadolinium-doped Ceria (CGO) composite electrocatalyst as a protective layer for a Solid-Oxide Fuel Cell anode fed with biofuels, ChemCatChem, 8 (2016) 648-655.

35. [35] M. Lo Faro, W. Oliveira da Silva, W. Valenzuela Barrientos, G.G.A. Saglietti, S.C. Zignani, E.A. Ticianelli, V. Antonucci, A.S. Aricò, The role of CuSn alloy in the co-electrolysis of CO2 and H2O through an intermediate temperature solid oxide electrolyser, Journal of Energy Storage, 27 (2020).
36. [36] M. Lo Faro, W. Oliveira da Silva, W.V. Barrientos, G.G.A. Saglietti, S.C. Zignani, V. Antonucci, E.A. Ticianelli, A.S. Aricò, Enhanced production of methane through the use of a catalytic Ni–Fe pre-layer in a solid oxide co-electrolyser, International Journal of Hydrogen Energy, 45 (2020) 5134-5142.
37. [37] G. Yang, W. Zhou, M. Liu, Z. Shao, Enhancing Electrode Performance by Exsolved Nanoparticles: A Superior Cobalt-Free Perovskite Electrocatalyst for Solid Oxide Fuel Cells, ACS Applied Materials and Interfaces, 8 (2016) 35308-35314.
38. [38] O. Kwon, S. Sengodan, K. Kim, G. Kim, H.Y. Jeong, J. Shin, Y.-W. Ju, J.W. Han, G. Kim, Exsolution trends and co-segregation aspects of self-grown catalyst nanoparticles in perovskites, Nature Communications, 8 (2017) 1-7.
39. [39] M. Lo Faro, R.M. Reis, G.G.A. Saglietti, V.L. Oliveira, S.C. Zignani, S. Trocino, S. Maisano, E.A. Ticianelli, N. Hodnik, F. Ruiz-Zepeda, A.S. Aricò, Solid oxide fuel cells fed with dry ethanol: The effect of a perovskite protective anodic layer containing dispersed Ni-alloy @ FeOx core-shell nanoparticles, Applied Catalysis B: Environmental, 220 (2018) 98-110.
40. [40] M. Lo Faro, V.L. Oliveira, R.M. Reis, G.G.A. Saglietti, S.C. Zignani, S. Trocino, E.A. Ticianelli, A.S. Aricò, Solid Oxide Fuel Cell fed directly with dry glycerol, Energy Technology, 7 (2019) 45-47.
41. [41] S. Vecino-Mantilla, E. Quintero, C. Fonseca, G.H. Gauthier, P. Gauthier-Maradei, Catalytic steam reforming of natural gas over a new Ni exsolved Ruddlesden-Popper manganite in SOFC anode conditions, ChemCatChem, 12 (2020) 1453-1466.
42. [42] R. Nishikawa, K. Kakinuma, H. Nishino, M.E. Brito, S. Gopalan, H. Uchida, Synthesis and Evaluation of Ni Catalysts Supported on BaCe0.5Zr0.3−xY0.2NixO3−δ with Fused-Aggregate Network Structure for the Hydrogen Electrode of Solid Oxide Electrolysis Cell, Catalysts, 7 (2017) 223.
43. [43] B.A. Rosen, Progress and Opportunities for Exsolution in Electrochemistry, Electrochem, 1 (2020) 32-43.
44. [44] M. Lo Faro, D. La Rosa, I. Nicotera, V. Antonucci, A.S. Arico, Electrochemical investigation of a propane-fed solid oxide fuel cell based on a composite Ni-perovskite anode catalyst, Applied Catalysis B-Environmental, 89 (2009) 49-57.
45. [45] M. Lo Faro, S. Campagna Zignani, A.S. Aricò, Lanthanum Ferrites-Based Exsolved Perovskites as Fuel-Flexible Anode for Solid Oxide Fuel Cells, Materials, 13 (2020).
46. [46] M. Lo Faro, V. Modafferi, P. Frontera, P. Antonucci, A.S. Aricò, Catalytic behavior of Ni-modified perovskite and doped ceria composite catalyst for the conversion of odorized propane to syngas, Fuel Processing Technology, 113 (2013) 28-33.
47. [47] M. Lo Faro, V. Antonucci, P.L. Antonucci, A.S. Aricò, Fuel flexibility: A key challenge for SOFC technology, Fuel, 102 (2012) 554-559.
48. [48] M. Lo Faro, A.S. Arico, Electrochemical behaviour of an all-perovskite-based intermediate temperature solid oxide fuel cell, International Journal of Hydrogen Energy, 38 (2013) 14773-14778.
49. [49] M. Lo Faro, S. Trocino, S.C. Zignani, V. Antonucci, A.S. Aricò, Production of syngas by solid oxide electrolysis: A case study, International Journal of Hydrogen Energy, 42 (2017) 27859-27865.
50. [50] M. Lo Faro, S.C. Zignani, S. Trocino, V. Antonucci, A.S. Aricò, New insights on the co-electrolysis of CO2 and H2O through a solid oxide electrolyser operating at intermediate temperatures, Electrochimica Acta, 296 (2019) 458-464.
51. [51] L. Bian, C. Duan, L. Wang, Z. Chen, Y. Hou, J. Peng, X. Song, S. An, R. O'Hayre, An all-oxide electrolysis cells for syngas production with tunable H2/CO yield via co-electrolysis of H2O and CO2, Journal of Power Sources, 482 (2021).
52. [52] M. Reisert, A. Aphale, P. Singh, Solid Oxide Electrochemical Systems: Material Degradation Processes and Novel Mitigation Approaches, Materials, 11 (2018) 2169.
53. [53] K. Zeng, D. Zhang, Recent progress in alkaline water electrolysis for hydrogen production and applications, Progress in Energy and Combustion Science, 36 (2010) 307-326.
54. [54] M. Torrell, S. García-Rodríguez, A. Morata, G. Penelas, A. Tarancón, Co-electrolysis of steam and CO2 in full-ceramic symmetrical SOECs: A strategy for avoiding the use of hydrogen as a safe gas, Faraday Discussions, 182 (2015) 241-255.

 doi:10.20944/preprints202012.0565.v1

55. [55] S. Hou, K. Xie, Enhancing the performance of high-temperature H2O/CO2 co-electrolysis process on the solid oxide Sr2Fe1.6Mo0.5O6-δ-SDC/LSGM/Sr2Fe1.5Mo0.5O6-δ-SDC cell, Electrochimica Acta, 301 (2019) 63-68.